Atmospheric
Measurement
Techniques

Characterization of trace metals on soot aerosol particles with the SP-AMS: detection and quantification

S. Carbone[1,a], T. Onasch[2], S. Saarikoski[1], H. Timonen[1], K. Saarnio[1], D. Sueper[2,3], T. Rönkkö[4], L. Pirjola[5,6], A. Häyrinen[7], D. Worsnop[1,2,5], and R. Hillamo[1]

[1]Atmospheric Composition Research, Finnish Meteorological Institute, P.O. Box 503, 00101 Helsinki, Finland
[2]Aerodyne Research, Inc. 45 Manning Road, 01821-3976, Billerica, MA, USA
[3]Cooperative Institute for Research In Environmental Sciences, University of Colorado, Boulder, CO 80303, USA
[4]Tampere University of Technology, Department of Physics, Tampere, Finland
[5]Department of Physics, University of Helsinki, P.O. Box 64, 00014 Helsinki, Finland
[6]Metropolia University of Applied Sciences, P.O. Box 4021, Helsinki, Finland
[7]Helen Ltd., 00090 Helen, Helsinki, Finland
[a]now at: Department of Applied Physics, University of São Paulo, São Paulo, Brazil

Correspondence to: S. Carbone (carbone@if.usp.br)

Abstract. A method to detect and quantify mass concentrations of trace metals on soot particles by the Aerodyne soot-particle aerosol mass spectrometer (SP-AMS) was developed and evaluated in this study. The generation of monodisperse Regal black (RB) test particles with trace amounts of 13 different metals (Na, Al, Ca, V, Cr, Mn, Fe, Ni, Cu, Zn, Rb, Sr and Ba) allowed for the determination of the relative ionization efficiency of each metal relative to black carbon (RIE_{meas}). The observed $RIE_{meas} / RIE_{theory}$ values were larger than unity for Na, Rb, Ca, Sr and Ba due to thermal surface ionization (TSI) on the surface of the laser-heated RB particles. Values closer to unity were obtained for the transition metals Zn, Cu, V and Cr. Mn, Fe, and Ni presented the lowest $RIE_{meas} / RIE_{theory}$ ratios and highest deviation from unity. The latter discrepancy is unexplained; however it may be related to problems with our calibration method and/or the formation of metal complexes that were not successfully quantified. The response of the metals to the laser power was investigated and the results indicated that a minimum pump laser current of 0.6 A was needed in order to vaporize the metals and the refractory black carbon (rBC). Isotopic patterns of metals were resolved from high-resolution mass spectra, and the mass-weighted size distributions for each individual metal ion were obtained using the high-resolution particle time-of-flight (HR-PToF) method.

The RIE_{meas} values obtained in this study were applied to the data of emission measurements in a heavy-fuel-oil-fired heating station. Emission measurements revealed a large number of trace metals, including evidence for metal oxides and metallic salts, such as vanadium sulfate, calcium sulfate, iron sulfate and barium sulfate, which were identified in the SP-AMS high-resolution mass spectra. SP-AMS measurements of Ba, Fe, and V agreed with ICP-MS analyzed filter samples within a factor of 2 when emitted rBC mass loadings were elevated.

1 Introduction

Trace metals are found in atmospheric aerosol particles from various combustion processes, such as vehicular emissions and industrial sources (Gao et al., 2002; Mbengue et al., 2014), and mechanical processes, such as wind-derived soil dust and sea salt (Pacyna 1998; Allen et al., 2001). Metals are frequently linked to adverse health effects; for instance, chromium, manganese and nickel are among the hazardous air pollutants listed by the EPA (EPA, 2005). There are several applications where the detection and quantification of trace metals are desirable. For example, trace elements have been used as tracers for certain emission sources: potassium

for biomass burning; vanadium and nickel for petrochemical plants and/or fuel-oil combustion; and iron, chromium, manganese, zinc and cadmium for steelwork and smelter emissions (Querol et al., 2007, Mbengue et al., 2014). Moreover, the detection of trace elements is useful in order to evaluate the engine performance in controlled engine emission experiments.

Several offline methods (e.g., X-ray fluorescence (XRF), proton-induced X-ray emission (PIXE), inductively coupled plasma mass spectrometer (ICP-MS)) have been previously used to determine trace metal concentrations in aerosol samples (Lough et al., 2005; Querol et al., 2007; Moffet et al., 2008). However, due to low concentrations in ambient aerosol, long sampling times (typically 24–72 h) have been necessary for offline trace metal analysis, hindering the investigation of short plumes or diurnal cycles. In that sense, online methods will provide clear improvement in trace metal analysis.

The aerosol time-of-flight mass spectrometer (ATOFMS) is one example of an online method which can detect trace elements in aerosol particles (Prather et al., 1994, Liu et al., 1997). However, the limited particle size range and detection efficiency of this instrument (0.3 % for 95 nm and 44.5 % for 290 nm particles; Su et al., 2004) resulted in a significant constraint for the mass quantification process. The design of the Aerodyne high-resolution time-of-flight aerosol mass spectrometer (HR-ToF-AMS) allows quantitative analysis of various chemical species, and it was used by Salcedo et al. (2012) to identify and quantify the trace elements copper, zinc, arsenic, selenium, tin and antimony in real time in Mexico City. Additional metals could not be detected due to the limitation of the maximum temperature reached by the vaporizer, typically 600 °C. Onasch et al. (2012) equipped the AMS with a laser vaporizer (soot-particle aerosol mass spectrometer, SP-AMS), which allowed refractory material such as soot to be vaporized and measured. Cross et al. (2012) and Dallmann et al. (2014) used the SP-AMS to detect the relative concentrations of trace elements Ca, Zn, Mg, and P in the emissions of a laboratory-based diesel engine and on-road diesel truck engines, respectively. Nilsson et al. (2015) used the SP-AMS to characterize metal nanoparticles (Ag, Au, Pd, Fe, Ni and Cu) in the aerosol phase.

The purpose of this study is to develop a method for the quantification of trace metal content in black carbon aerosol, such as combustion-related emissions, by using the SP-AMS. In combustion related emissions black carbon and trace metals are co-emitted, and the latter will exist on the black carbon aerosol particles. The properties of 13 different trace metals (Na, Al, Ca, V, Cr, Fe, Mn, Ni, Cu, Zn, Rb, Sr and Ba) were investigated in a controlled laboratory experiment in order to measure their relative ionization efficiencies. The results from the laboratory tests were applied to study fine particles in emissions of a heavy-fuel-oil-fired heating station.

2 Experimental

2.1 Instrumentation

2.1.1 Soot-particle aerosol mass spectrometer (SP-AMS)

The online chemical composition of submicron particles was measured by using a soot-particle aerosol mass spectrometer (Aerodyne Research Inc., USA; Onasch et al., 2012). The SP-AMS is a combination of two well-characterized instruments: the Aerodyne HR-ToF-AMS (Aerodyne Research Inc. MA, USA; DeCarlo et al., 2006) and the single-particle soot photometer (SP2, Droplet Measurement Technologies, CO, USA; Stephens et al., 2003). In the HR-ToF-AMS, an aerodynamic lens is used to form a narrow beam of particles that is transmitted into the detection chamber where aerosol components are flash-vaporized upon impact on a hot tungsten surface (600 °C) under high vacuum (Jayne et al., 2000). Only non-refractory species are rapidly vaporized at this temperature. The vaporized compounds are subsequently ionized using electron impact ionization (70 eV) and guided to the time-of flight mass spectrometer. In the SP-AMS, an intracavity Nd : YAG laser vaporizer (1064 nm), based on the design used in the SP2 instrument, was incorporated into the HR-ToF-AMS. The addition of a laser vaporizer enabled the vaporization and detection of light-absorbing refractory particles, specifically refractory black carbon (rBC). The laser vaporizer does not interfere with the standard tungsten vaporizer used in the HR-ToF-AMS instrument or generate chemical ions. Therefore, the SP-AMS instrument can be operated with the laser vaporizer alone, with both the laser and tungsten vaporizers, or just with the tungsten vaporizer. When operated with both vaporizers, the laser is modulated on and off in order to measure rBC and associated less refractory particulate material in addition to the standard AMS non-refractory species (sulfate, nitrate, ammonium, chloride, organics). In this study, the SP-AMS had both the tungsten and the laser vaporizer operating at the same time. The sampling time for the SP-AMS was set to 30 seconds. The sample time of the SP-AMS was split 50 : 50, measuring mass spectra (MS mode: mass loading concentrations without particle size information) and mass-weighted size distributions (PTOF mode). During this experiment, the collection efficiency was assumed to be unity (CE = 1).

2.1.2 Other instruments

Additional instruments were utilized during the laboratory experiments. The constant output atomizer (TSI model 3076) was operated at a constant pressure (∼ 2 bar). The differential mobility analyzer (DMA, TSI model 3080) operated at 10 L min^{-1} sheath air, and the condensation particle counter (CPC, TSI model 3772) at 1 L min^{-1} of aerosol. A silica gel drier (TOPAS; length 25 cm) and a sonic probe (ultrasonic

cleaner Branson 200) were used in order to dry the aerosol particles and promote the dispersion of the components, respectively.

In the field experiments, a comprehensive setup was used. More detailed information on the setup is given in Frey et al. (2014). Briefly, the exhaust from the oil burner was first diluted using filtered air and then studied for particles with online instrumentation and using sample collection for subsequent chemical analysis. Dilution ratios were calculated on the basis of measured CO_2 concentrations in the raw flue gas and in the diluted sampled air. The offline analysis methods included a NanoMOUDI cascade impactor (model 125B), allowing for the collection of size-segregated particles in the size range of 10 nm–10 μm. Inductively coupled plasma–mass spectrometry (ICP-MS) was used to determine trace metal concentrations from the size-segregated NanoMOUDI substrates.

2.2 Standards and solutions

Stock solutions of 13 different metals (Na, Al, Ca, V, Cr, Fe, Mn, Ni, Cu, Zn, Rb, Sr and Ba in 2 % nitric acid, Sigma-Aldrich), Regal black (RB, REGAL 400R pigment black, Cabot Corp.) and deionized water were used to make the calibration standard solutions for the laboratory experiments. The exact mass concentrations of each trace metal standard, as well as the relative atomic mass and isotopic compositions, are depicted in Table S1 in the Supplement.

The stock metal solutions were used to make one standard metal solution containing 1×10^{-6} kg of each metal and filled to 0.1 L with deionized water (concentration of 1×10^{-5} kg L^{-1}). The quantification experiments occurred in several steps, including a blank and eight varying solution concentrations for each metal. In the blank step, only the RB was atomized and measured (2.4×10^{-5} kg of RB in 0.2 L of deionized water, concentration of 1.2×10^{-4} kg L^{-1}; this concentration was kept constant throughout the experiment). During this step, the RB sample was tested for the detection of each of the 13 metals of interest, before the addition of any metal, to rule out potential contamination. From the metals evaluated in this study, only Na exhibited a measureable background concentration (less than 0.1 %). The other metals were not detected, indicating background concentrations of metals in the original RB below the limit of detection. In the following steps, a given standard metal solution was added to the RB solution gradually (1×10^{-3} L per step), increasing the metal content. As a result, the amount of each metal in the atomized solution varied between 0 and 8×10^{-8} kg. SP-AMS measurements were done at every step. The RB was used as a carrier for the trace metal concentrations and as a light-absorbing material detectable by the laser vaporizer employed in the SP-AMS, which is optimal for black carbon vaporization (1064 nm). The RB chemical ion signal measured by the SP-AMS is called rBC and is the sum of the C_1^+ to C_5^+ carbon cluster ions. The trace metals were

quantified in the laboratory experiments relative to the carrier rBC mass loadings (i.e., relative ionization efficiencies). Using this method, the absolute collection efficiency for rBC particles in the SP-AMS laser vaporizer is not required. In ambient measurements, the detection of metals in aerosol particles containing rBC is important as they are generated and co-emitted by many different combustion sources; both components are important for local, regional and global climate and pollution issues, and both exhibit adverse impacts to human health (Ramanathan and Carmichael, 2008; Dockery, 2001).

2.3 The method to measure metal concentrations

The key point for determining the quantitative metal mass concentrations with the SP-AMS is to measure the value of the relative ionization efficiency (RIE$_{meas}$) of each metal, that is, the ionization efficiency of the metal compared to the ionization efficiency of a calibration material (i.e., nitrate or rBC). The measured RIE values (RIE$_{meas}$) were then compared with the RIE values derived from the literature (RIE$_{theory}$). When the ratio RIE$_{meas}$ / RIE$_{theory}$ approaches unity, the method was assumed to be well represented by the theory and the method suitable for quantitative metal detection. The following sections describe the generation of aerosol particles in the laboratory and the estimation of the RIE values (RIE$_{meas}$ and RIE$_{theory}$).

2.3.1 Aerosol particle generation

Polydisperse submicron aerosol particles were generated by the atomizer from different solutions containing RB, water, and trace metals (and small amounts of nitric acid from the stock metal solutions). The sonic probe was used to provide constant dispersion of the components (RB and metals) in the solvent (water). After the atomizer, particles were passed through the silica gel drier and directed into the DMA. The DMA generated monodisperse (300 nm, mobility diameter) aerosol, which was split between the CPC (1 L min^{-1}) and the SP-AMS (0.1 L min^{-1}). A schematic diagram of the setup used is shown in the Supplement (Fig. S1).

2.3.2 Relative ionization efficiency estimates

The RIE value of the species s (RIE$_s$, relative to nitrate) and a nitrate calibration is required in order to convert the signal of a specific ion measured by the SP-AMS (Hz) into mass concentration (μg m^{-3}) (Eq. 2 in Onasch et al., 2012). In this study, the RIE of each metal ion was obtained relative to rBC (where C_3^+ was used as a surrogate of rBC), instead of nitrate, because the rBC is the calibration standard for the laser vaporizer in the SP-AMS.

To estimate the theoretical RIE for a given metal (RIE$_{theory}$), the values of the ionization efficiency for each species (IE$_s$) and molar weight (MW$_s$) are needed (Eqs. 3 and 4 in Onasch et al., 2012), which are not easily found in

the literature. For that reason, Jimenez et al. (2003) proposed that the value of IE_s of an ion or molecule is directly proportional to the electron impact ionization cross section (σ), and the number of electrons in an ion or molecule (Ne) is approximately proportional to its molar weight (MW). The values of σ are available in the literature (Table 2), and Ne can be determined once the ion is known. Hence, the RIE_{theory} was obtained through the ratio σ_s / Ne_s as described in Eq. (1), where M represents one metallic ion.

$$RIE_{theory} = \frac{\sigma_M}{Ne_M} \bigg/ \frac{\sigma_{rBC}}{Ne_{rBC}} \tag{1}$$

To measure the values of the RIE of each metal measured by the SP-AMS (RIE_{meas}), we assumed that the ratio of the mass of each dissolved metal to the suspended RB particles was the same in the size-selected, dry particles as in the atomized solution. We used only trace amounts of metals and high RB mass concentrations in the solution in an attempt to ensure that all of the metal was associated with RB particles. While we did not definitively test the validity of this assumption, the linearity of the measured metal ion signals relative to the calculated metal mass loadings (Fig. S3) and the comparisons of the RIE_{meas} vs. RIE_{theory} (discussed in Sect. 3.1.5) provide indirect support. Based on this assumption, the number concentration of particles measured by the CPC was converted into rBC mass assuming monodisperse particles (300 nm, mobility diameter, d_m) with an effective density (the mass is divided by the volume of a sphere with the same mobility diameter d_m) of RB (900 kg m^{-3}) (Onasch et al., 2012). This was called the CPC mass method. Thus, the mass of each metal was calculated as shown in Eq. (2):

$$m_M = Z \times m_{rBC}, \tag{2}$$

where m_M and m_{rBC} represent the mass in micrograms per cubic meter (μg m^{-3}) of M and rBC, respectively, and Z represents the mass fraction of the metal relative to the RB in the solution. For instance, in this experiment Z varied between 0 and 0.32 %, as the metal solution was added to the RB solution gradually (0–8×10^{-3} L). Because of the small fraction of metals relative to RB in the solution, it is assumed that the particles were mainly composed of the RB and the metals were attached to its surface or interior. The measured RIE for each metal is discussed in more detail in Sect. 3.1.5.

2.3.3 Thermal surface ionization

The surface ionization (SI) takes place when an atom or molecule is ionized due to the interaction with a solid surface, and it is dependent on the work function and temperature of the surface and the energy required by each atom or molecule to be ionized (Todd, 1991). If the surface is heated, that process is also referred to as thermal ionization (Todd, 1991). In this study the surface ionization on a heated surface will be called thermal surface ionization (TSI).

TSI was first reported in the Aerodyne AMS by Allan et al. (2003) with K$^+$ ions formed at the heated surface (~ 600 °C) of the tungsten vaporizer. In general, this type of ionization is undesirable because (1) it produces ions with a significantly different efficiency (typically orders of magnitude higher) than standard electron-impact (EI) ionization and (2) it produces ions with different energies associated than the ones produced by the EI ionization. In practice, TSI may cause a distortion in the ion peak shape detected by the instrument, further complicating the mass quantification process by the SP-AMS.

In order to investigate the possibility of TSI, a qualitative experiment was carried out in the laboratory. The SP-AMS was operated with the laser vaporizer on, but with the tungsten vaporizer turned off and the EI filament current set to 0. Under these conditions, the soot particles are still heated to vaporization temperatures (~ 4000 °C) via absorption of the laser vaporizer power, but measured ions must be generated by mechanisms other than EI ionization, such as TSI. Under these experimental conditions, we sampled RB particles coated with a mixture of all 13 metals; the results obtained in this experiment will be discussed in the results section.

2.4 Field measurements

Field measurements were carried out in an oil-fired heating station in Helsinki, Finland, from 12 to 15 December 2011. Besides the SP-AMS, several different instruments measured the emissions from three different boilers that burned different combinations of heavy fuel oil and light fuel oil with or without water as an emulsion. Further information concerning the instrument setup and measurements were presented in Happonen et al. (2013) and Frey et al. (2014).

3 Results and discussions

3.1 Results of the method development

3.1.1 Identification of metals with isotopic patterns

The identification of metals was performed by using their exact m/z ratios and by investigating their isotopic patterns. However, the low signal observed for several isotopes, due to their low isotopic composition, prevented the determination of some of the isotopes. Barium was used as an example here, since it had the best signal. For instance, the isotopes ^{134}Ba, ^{135}Ba, ^{136}Ba, ^{137}Ba and ^{138}Ba corresponded to 99.79 % of the Ba total mass, where ^{138}Ba itself represented 71.69 % (Watson et al., 2004); see Table 1. The isotopic compositions (ICs) were evaluated relative to the most abundant isotope (^{138}Ba), and the relative isotopic compositions (RICs) obtained by the SP-AMS were compared to the reference RIC (Watson et al., 2004). The agreement varied from 58 to 96 %; i.e., the ratio of ^{137}Ba to ^{138}Ba measured with the SP-AMS represented 96 % of the reference ratio value (Ta-

Table 1. Isotopic composition (IC) and relative isotopic composition (RIC) according to NIST database and measured with the SP-AMS.

Element	IC (%)*	RIC*	Measured RIC
^{138}Ba	71.69	1.00	1.00
^{137}Ba	11.23	6.38	6.18
^{136}Ba	7.85	9.12	8.08
^{135}Ba	6.59	10.87	10.22
^{134}Ba	2.41	29.66	17.24

* Watson et al. (2004).

ble 1), while the measured ratio of ^{134}Ba to ^{138}Ba represented only 58 % of the reference ratio value. The disagreement for ^{134}Ba was probably due to the low signal of this ion (2.4 % of ^{138}Ba signal and below 1 Hz). In addition, the signal of the different isotopes showed clear linear variation with the signal of ^{138}Ba; the linear correlations (r^2, Pearson correlation) varied from 0.68 to 0.91 (Fig. 1). A complete list of the elements and respective isotopes identified in this study can be found in the Supplement (Table S1).

3.1.2 Size distributions

The size distributions of metals were investigated in order to validate the performance of the particle generation system. Size distributions were calculated by using the algorithm implemented in Squirrel version 1.52L and Pika version 1.11L AMS analysis software (Sueper, 2008, http://cires.colorado.edu/jimenez-group/ToFAMSResources/ToFSoftware/) for each individual ion measured by the SP-AMS (hereafter called HR-PToF: high-resolution particle time-of-flight). The average mass HR-PToF size distributions of different mobility size-selected and dried RB particles with trace metals ^{51}V, ^{52}Cr, and ^{88}Sr$^+$ are presented in Fig. 2. The signal intensity of rBC as a function of size was estimated based on its mass spectrum, which was composed of 27.6 % C_1^+, 15.8 % C_2^+, 44.3 % C_3^+, 3.8 % C_4^+ and 4.8 % C_5^+. The sum of C_1^+–C_5^+ represented 96 % of the total rBC ion signal. The results depicted a clear unimodal size distribution for all the metals and the rBC centered at 230 nm (vacuum aerodynamic diameter, d_{va}), corresponding to the selected 300 nm mobility diameter. The conversion from mobility diameter to d_{va} has been previously described by DeCarlo et al. (2004) and depends on the shape and density of the particles.

3.1.3 The effect of the laser power

The response of the metals and rBC to the laser power was also studied. Here, the pump laser current worked as an indicator of the intracavity laser power. Increasing gradually from zero, there was a clear increase in the signal of all the metals and rBC ions when the current was set to 0.4 A. How-
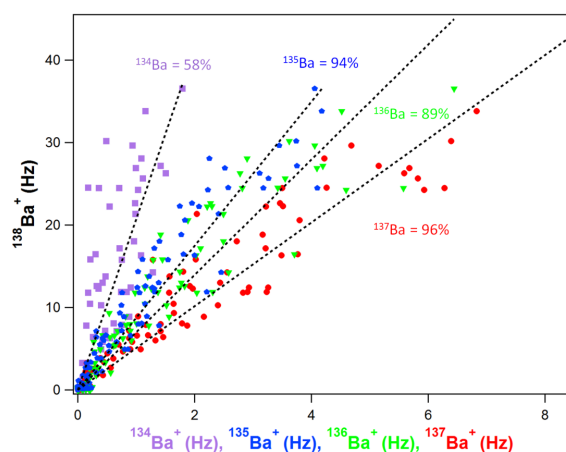
Figure 1. Barium isotopic pattern measured in the laboratory. The percentages correspond to the isotopic compositions relative to the most abundant (^{138}Ba$^+$).

ever, the value of 0.4 A was likely not enough to fully vaporize the rBC (about 60 mW according to Onasch et al., 2012). At that current, most of the metals reached their maximum signal immediately, whereas for rBC current up to 0.6 A was needed to reach its maximum signal. This fact indicated that all the other species were more volatile than rBC, which requires about 4000 °C to evaporate. After this threshold current (0.4 A for metals and 0.6 A for rBC), the increase in current did not increase the signal, and any current below the threshold (0.6 A) is not suitable for vaporization of particles containing rBC and metals. All metals presented close to zero ion signal (< 1 %) when the laser was operated below 0.4 A; rBC was also below 1 % (Fig. 3). The only exceptions were nitrate and ammonium. The presence of those ions under the condition of very low laser power suggested the presence of ammonium nitrate salt (10 % of the rBC signal), derived from the nitrate in the stock metal solutions and trace ammonia in the filtered sample air, which was vaporized by the tungsten vaporizer. Note that the signal fractions displayed in Fig. 3 were obtained in ion signal (Hz), not in mass concentration (µg m^3).

3.1.4 Thermal surface ionization

In order to study the TSI effect, the SP-AMS was operated with the laser vaporizer turned on, the tungsten vaporizer turned off, and the EI filament current set to 0. Under these conditions, the ions Cr$^+$, V$^+$, Ca$^+$, Al$^+$, Sr$^+$, Ba$^+$, Na$^+$ and Rb$^+$ (here in descending order of ionization energy) and their respective isotopes were identified in the mass spectrum of the SP-AMS (Fig. S2). Because the tungsten vaporizer was cold (< 100 °C) and the rBC concentration was abundant, it is hypothesized that these ions were generated on the hot surface of the rBC via TSI. Therefore, EI ionization was not the only process responsible for ionization of these metals. In
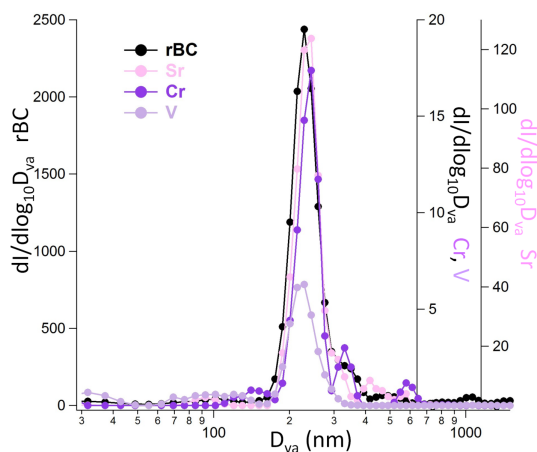
Figure 2. High-resolution signal intensity size distributions (HR-PToF) of rBC, V^+, Cr^+ and Sr^+.

Figure 3. Fraction of metals signal (Hz) relative to the highest rBC signal (Hz) as a function of the laser diode current (LDC).

fact, in the case of the ions mentioned above, the TSI was very significant in determining the apparent mass concentrations. As discussed in Sect. 2.3.3, apparent RIEs of metals with ions formed via TSI and EI will be overestimated and hinder quantification of these metals in the SP-AMS. In addition to the eight metals mentioned above, potassium (K) was also present in the mass spectrum (Fig. S2, with same isotopic composition verified by the NIST database $^{41}K/^{39}K = 7\%$). Because this metal was not present in the solutions used in this experiment, it was likely due to contamination. The probability for TSI is described by the Saha–Langmuir equation (Zandberg and Ionov, 1971). Emission of positive ions is favored when the ionization potential of the desorbing atom or molecule is similar in magnitude or lower than the work function of the surface. In this experiment, assuming the particle surface consists of RB (a carbon black material), its work function might be similar to highly oriented pyrolytic graphite (HPOG), which has a work function value of 4.6 eV (Shiraishi et al., 2001). In fact, the RB work function might actually be larger than that of HPOG as RB is advertised by its manufacturer as an oxidized carbon black and the work functions of commercially available carbon blacks increase with increasing acidity and oxidation of the surface (Fabish and Hair, 1977). In this laboratory study, nitric acid was present inside the stock metal solutions, which could have further increased the work function of RB. A relatively high work function value for RB (~ 5.1 eV) would be in agreement with our observations of multiple metals undergoing TSI in the SP-AMS. The key comparison in this case is the number of ions generated by TSI, estimated from the Saha–Langmuir equation, compared with the number of ions generated by EI for a given metal, which is estimated using the theoretical approached described in Sect. 2.3.2.

In ambient measurements, the work function of rBC particles is probably also higher than that of HPOG. For example, combustion processes, such as from industrial sources,
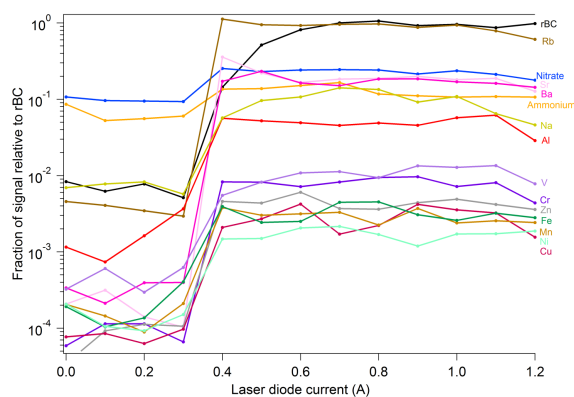
may emit organic compounds, such as hydrocarbons and acids, which attached to the co-generated rBC particles. Ago et al. (1999) showed that the presence of additional surface functional groups containing oxygen increased the work function of carbon nanotubes. Thus, ambient rBC particles likely have a work function that may be closer to that of RB than HPOG. Under these conditions, TSI may be a significant interference to the ability of SP-AMS to quantify these trace metals on ambient rBC particles.

3.1.5 Relative ionization efficiency of metals

Measured relative ionization efficiency

The ion signal of each metal measured by the SP-AMS (in Hz) was plotted as a function of the mass obtained by the CPC method (Eq. 2) for all the different concentrations of the metals in the atomized solutions. The slope from this comparison (α_M) was then divided by the slope obtained from the rBC mass calibration (β_{rBC}), which was performed before the current experiment under the same conditions. The rBC calibration process was performed as described by Onasch et al. (2012). The ratio of the two slopes represented the value of the ionization efficiency of the metal M measured relative to the rBC (Eq. 3) (RIE_{meas}, Fig. 4). The measured ion signals by the SP-AMS (Hz) as a function of the mass concentration obtained by the CPC (μ g m^{-3}) for each individual metal and respective slopes are available in the Supplement (Fig. S3).

$$RIE_{meas} = \frac{\alpha_M}{\beta_{rBC}} \qquad (3)$$

Measured vs. theory

The ratio $RIE_{meas} / RIE_{theory}$ enables the evaluation of the performance of the method suggested in this study (Table 2). Values much larger than unity were obtained for the alkali Na, Rb, and Ca (the isotope ^{42}Ca was used to estimate ^{40}Ca due to interference of Ar at m/z 40) and the alkaline earth
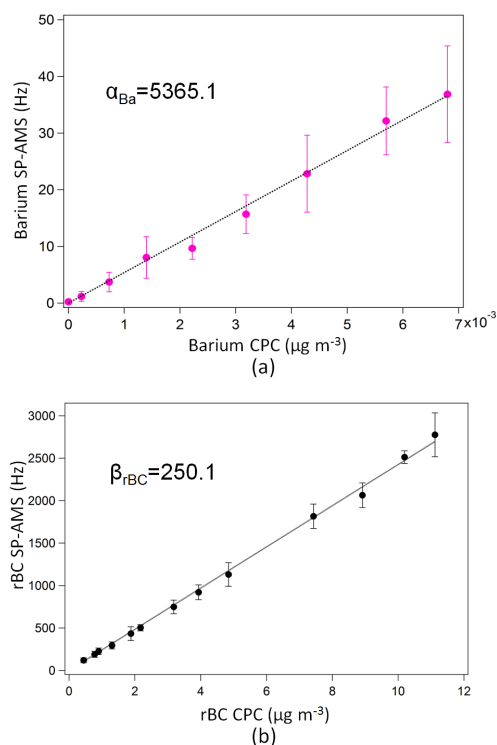
Figure 4. Signal measured by the SP-AMS (Hz) versus the mass concentration obtained by the CPC ($\mu g\,m^{-3}$) for barium **(a)** and rBC **(b)**.

metals Sr and Ba. These metals have lower ionization potentials and therefore are more susceptible to being surface-ionized, as already described in the previous section. Values closer to unity were obtained for Al, V, Cr and Zn (C_3^+ was equal to unity because it was used as a reference), which indicated that the measured RIE for those metals was similar to the theoretical value and that the method used here was suitable for quantification. The transition metals Mn, Fe and Ni presented the lowest ratio and highest deviation from unity (0.36, 0.47 and 0.28, respectively). We currently do not have a conclusive explanation for this discrepancy. Losses may have occurred at three stages: (1) losses in the atomizer, where the mass ratio of the metal to rBC was not kept constant despite our best efforts; (2) formation of side products, such as metallic oxides or salts, which were not quantified during the RIE experiments; and (3) losses in the laser vaporizer due to the high temperature required to evaporate certain metals or metal-containing compounds. The laser vaporizer beam in the SP-AMS does not fully overlap the particle beam. That is, the metals that require higher temperatures to evaporate were only vaporized when positioned close to the center of the laser beam, the position where the temperature is the highest ($\sim 4000\,°C$). At the borders of the laser beam only metals that required lower temperatures were vaporized.

A comprehensive list containing all the metal-containing ions and their respective fragments, which we might expect to observe during our laboratory experiments, was added to the Supplement (Table S2). From this list, 20 metallic fragments containing oxygen and nitrogen in the form of metallic salts (nitrites, nitrates and nitrides) and oxides were positively identified in our laboratory mass spectra. Most of these ions could only be detected when the metal solutions were at their highest concentration levels, suggesting that their concentrations were a small fraction of the total ion signal detected for a given metal sample. The three exceptions were the fragments $MnNO^+$, $FeNO^+$, and $NiNO^+$, which were observed at several steps of the RIE laboratory experiments. While we were unable to quantify these metal complex ions, it is possible that some of the difference in the RIE ratios observed for Mn, Fe and Ni was due to formation of these side products.

The measured RIEs of each metal M relative to rBC ($RIE_{M,rBC}$) need to be converted into RIEs relative to nitrate in order to implement those values of RIE_M into the AMS analysis software Pika (Sueper, 2008). The conversion can be achieved by simply multiplying the obtained RIE_M relative to rBC ($RIE_{M,rBC}$) by the RIE of rBC relative to nitrate ($RIE_{rBC,nitrate}$), as shown in Eq. (4). For example, RIE for V^+ ($RIE_{V,rBC}$) obtained in this study was 1.36 (Table 2), and the RIE of rBC (now relative to nitrate, $RIE_{rBC,nitrate}$) was 0.56; therefore the $RIE_{V,nitrate}$ value to be implemented into Pika is 0.76.

$$RIE_{M,\ nitrate} = RIE_{rBC,nitrate} \times RIE_{M,rBC} \qquad (4)$$

Note that Eq. (4) indicates that $RIE_{M,nitrate}$ will be dependent on the value of the $RIE_{rBC,nitrate}$, which means that this value must be known. This value was measured here to be 0.56 and proposed by Onasch et al. (2012) to be 0.2 ± 0.1, which can be used in studies where it is not possible to measure it.

The $RIE_{rBC,nitrate}$ may be affected by different potential ionization efficiencies between the laser vaporizer and the tungsten vaporizer, which is discussed in more detail by Lee et al. (2015). In particular, the two vaporizers (1) generate neutral plumes in different regions of the ion chamber and (2) generate neutral plumes with different molecular velocities, both of which could lead to different ionization efficiencies. Since the temperature of the tungsten vaporizer is typically operated at $600\,°C$ and the carbon vaporizers from rBC materials typically operate at $\sim 4000\,°C$, these different materials will have different kinetic energies during evaporation and the carbon clusters may spend less time in the ionization chamber, leading to lower ionization efficiencies.

Despite these apparent discrepancies between the ionization efficiencies from the laser vaporizer (rBC) and tungsten vaporizer (nitrate), we expect the ionization efficiencies of metal and rBC generated from vaporization in the laser vaporizer to be more similar with respect to (1) neutral plume location and (2) neutral velocities.

Willis et al. (2014) measured the CE of bare RB particles and estimated a value of 0.6 for irregularly shaped particles. The irregular shape leads to divergence in the particle beam

Table 2. Metallic ions evaluated in the laboratory experiment, electron impact cross section (σ), theory relative ionization efficiency (RIE_T), measured relative ionization efficiency (RIE_M), relative ionization efficiency ratio (RIE_T / RIE_M) and limit of detection.

Ion	σ (A^2) (70 eV)	Boiling point (°C)	RIE_{theory}	RIE_{meas}	RIE_{meas} / RIE_{theory}	LD (ng m^{-3})
Na$^+$	2.01[a]	879	0.77	20.30	26.36	51
Al$^+$	7.82[b]	2518	2.50	5.02	2.01	30
Ca$^+$	5.80[c]	1494	1.17	287.50	245.23	87
V$^+$	7.20[d]	3380	1.26	1.36	1.08	26
Cr$^+$	7.50[e]	2672	1.25	0.97	0.77	21
Mn$^+$	6.80[d]	2051	1.09	0.40	0.36	117
Fe$^+$	4.38[b]	2835	0.67	0.32	0.47	87
Ni$^+$	6.20[d]	2732	0.88	0.25	0.28	111
Cu$^+$	3.75[d]	2567	0.51	0.43	0.83	90
Zn$^+$	5.60[d]	908	0.74	0.73	0.99	n/a
Rb$^+$	7.20[e]	688	0.77	158.47	206.34	10
Sr$^+$	8.20[c]	1384	0.85	23.19	27.24	10
Ba$^+$	10.50[c]	1140	0.73	21.42	29.23	11
C$_3^+$	4.43[f]	4000	1	1	1	13[g]

[a] Fujii and Srivastava (1995), [b] Freund et al. (1990), [c] Vainshtein et al. (1972), [d] Lotz (1970), [e] Kim et al. (1998), [f] Naghma and Antony (2013), [g] LD value estimated for rBC.

width, such that particles at the edges of the particle beam do not intersect the laser beam. Coated RB particles result in more spherical particles, which exhibit narrower particle beams with better laser beam overlap (Cross et al., 2010; Onasch et al., 2012; Willis et al., 2014). In this laboratory study, RB was coated by metals, albeit in very small content. Therefore, it is likely that these particles exhibited a CE more similar to bare RB. However, when measuring metal ionization efficiencies relative to rBC (i.e., RIE_{meas}), the absolute collection efficiencies for rBC particles in the SP-AMS laser vaporizer is not required.

3.2 Results of the field application

3.2.1 Measurements in an oil-fired heating station

Field measurements in an oil-fired heating station in Helsinki, Finland, were accomplished from 12 to 15 December 2011. The average mass spectrum during one of the operating conditions (mixture of light and heavy fuel oil, and water as emulsion with power of 47 MW) indicated the presence of rBC, organics, sulfate and metals (Na, Mg, K, Ca, V, Cr, Fe, Ni, Cu, Zn, Rb, Sr, Sb, Cd and Ba) in the emissions, shown in Fig. 5. When studied in more detail, the HR mass spectra indicated the presence of less typical fragments, such as aluminum silicate (Al_2SiO_5), metallic oxides (fragments ZnO_2^+, CaO^+, CrO^+, FeO^+) and the metallic salts (fragments $VOSO^+$, $VOSO_2^+$, $CaSO_2^+$, $FeSO_4^+$ and $BaSO_2^+$, Fig. 6). Metals and metallic sulfates present a clear negative mass defect, shown in Fig. 5. This fact facilitates their identification and quantification. In ambient measurements, sulfate is typically found in the form of ammonium sulfate (if neutralized) instead of metallic salts. In this experiment,

ammonium sulfate formation is unlikely due to the reduced amount of ammonium. The presence of elevated concentrations of sulfate and reduced concentrations of ammonium were confirmed by the SP-AMS and parallel ion chromatography analysis of the filter samples (Frey et al., 2014).

3.2.2 Sulfate fragmentation pattern

Fragmentation in the AMS instruments results from the thermal vaporization and 70 eV EI ionization processes employed, where sulfate main fragments correspond to the ions SO^+, SO_2^+, SO_3^+, HSO_3^+ and $H_2SO_4^+$. It has been observed that, in an ambient environment where the sulfate was mainly in the form of ammonium sulfate, the last four fragments as a function of SO^+ presented constant slopes for each AMS instrument (Allan et al., 2004).

In this field study, the slopes of those fragments (SO^+, SO_2^+, SO_3^+, HSO_3^+ and $H_2SO_4^+$) as a function of SO^+ were observed to vary with rBC and trace metal mass loadings (Fig. 7). In the vaporization process, the tungsten and laser vaporizer may transfer different internal energies to the vapors, which may cause different EI fragmentation patterns (Alfarra et al., 2004; Onasch et al., 2012). Because the SP-AMS had both vaporizers employed (switching the laser on/off), two distinct slopes may be expected for each fragment as a function of SO^+. In this field study, at least three distinct slopes were found. For example, the fragment SO_2^+ as a function of the SO^+ presented slopes (α) that ranged from 1.02 to 1.27. Conversely, the slopes of the fragments SO_3^+, HSO_3^+ and $H_2SO_4^+$ as a function of SO^+ presented values that ranged from 0.12 to 0.3, 0.11 to 0.31 and 0.05 to 0.17, respectively (Fig. 7). In practice, the presence of multiple slopes could be an indication of the sulfate aerosol par-
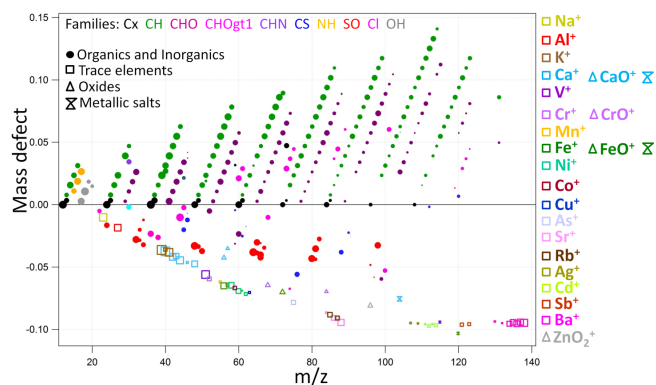
Figure 5. Mass defect (difference between the ion's exact mass and its nominal mass) obtained from the emissions of a heavy-fuel-oil power plant; the size of the marker is proportional to the square root of the signal of each ion. Organic and inorganic ions are represented with circles, metals with squares, oxides with triangles, and metallic sulfates with double triangles.

Figure 6. Average high-resolution mass spectra for the m/z 115 (**a**), 131 (**b**), 104 (**c**) and 120 (**d**) during the field experiment at the heating station.

ticles in the form of metallic sulfates, as was illustrated by Figs. 5 and 6. However, those slope values should not be interpreted as numeric indicators because different instruments could present different values due to intrinsic instrumental characteristics, such as ionizer and vaporizer design and configuration.

For comparison, measurements solely with the tungsten vaporizer were depicted together with the measurements with both vaporizers (Fig. 7). Under very low rBC loads, similar slopes were obtained for the different vaporizing techniques, which means that the laser vaporization did not take place. This fact is further discussed in the next section.

3.2.3 Mass concentrations and comparison with ICP-MS

The RIE_M values obtained in this study were implemented in Pika v. 1.11L, and the trace metal concentrations were calculated for the field measurements at the oil-fired heating station with the SP-AMS. Besides the SP-AMS, offline samples were collected using a NanoMOUDI cascade impactor (stages 6–13 corresponding to AMS size range) and analyzed with the ICP-MS method. Fig. 8 illustrates the measurements of the metals Fe (the sum of ^{56}Fe, ^{57}Fe and ^{58}Fe), V (^{51}V) and Ba (the sum of ^{134}Ba, ^{135}Ba, ^{136}Ba, ^{137}Ba and ^{138}Ba) by the SP-AMS in micrograms per cubic meter ($\mu g\,m^{-3}$) using the values of RIEs obtained in this study (Table 2) averaged into the filter sampling times analyzed with the ICP-MS (in $\mu g\,m^{-3}$).

The comparison presented better agreement (within a factor of 2) between the two techniques for the periods when rBC concentrations were elevated. Larger disagreement between the two techniques occurred in the periods when rBC was very low. Although the volume size distributions measured by ELPI (Electrical Low Pressure Impactor) (Fig. 3;
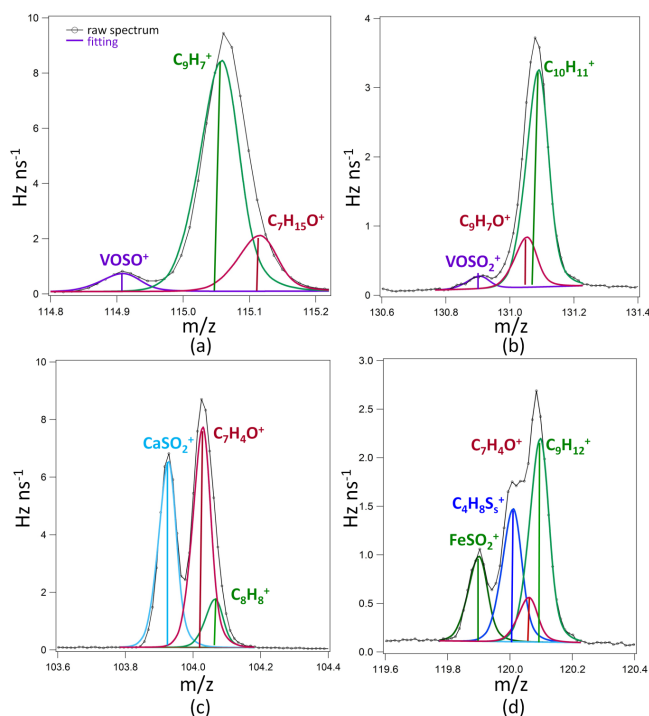
Happonen et al., 2013) indicated that only one mode was present in the size range of the SP-AMS, suggesting that rBC and metals were internally mixed in the same size range, it is possible that not all of the particles contained rBC material (i.e., not all particles are soot particles). If the latter case is true, then the SP-AMS sensitivity drops as the rBC mass fraction decreases due to more of the metals residing on non-rBC particles.

In addition, the clear evidence of oxides and metallic salt formation (Figs. 7 and 8) in periods of high rBC loads may lead to an underestimation of the metals by the SP-AMS, while the ICP-MS method determines the total metal content in the sample. If, on the one hand, the detection of trace metals with the SP-AMS relies on the presence of rBC-containing particles, on the other it consists of a real-time measurement technique, which allowed for the observation of fast changes in chemical composition of metallic compounds during combustion processes. Moreover, the SP-AMS provides further information on the identification of metal-containing compounds such as minerals, salts and oxides of soot-containing aerosol particles.
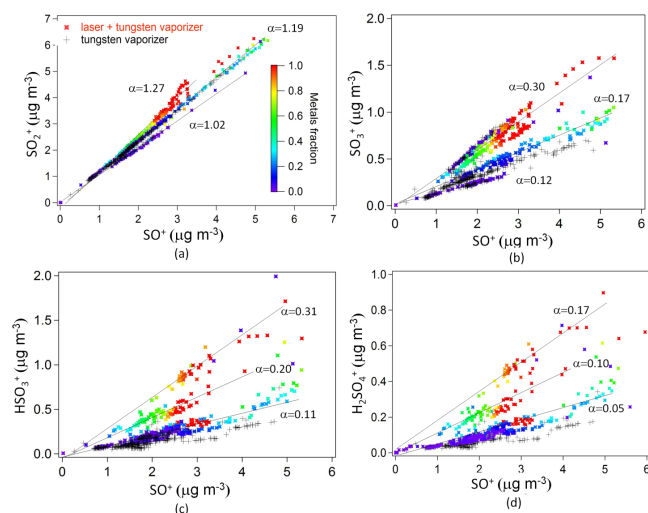
Figure 7. Sulfate fragmentation patterns, SO_2^+ vs. SO^+ (a), SO_3^+ vs. SO^+ (b), HSO_3^+ vs. SO^+ (c) and H_2SO^{4+} (d) during the field experiment at the heating station. For comparison, the black crosses represent the measurements solely with the tungsten vaporizer.

3.2.4   Sensitivity

The presence of rBC in the aerosol particles is essential to detect trace metals with the SP-AMS laser vaporizer. Metals associated with the rBC will be evaporated with the 1064 nm wavelength laser and detected. This fact was verified with the measurements at the heating station, by a clear dependence of the metals (sum of all the metals) on the rBC concentrations; i.e., the larger the rBC mass loadings, the larger the SP-AMS measured metal concentrations (Fig. 9). The different ratios between metals and rBC during the measurements were likely caused by the different conditions during the combustion (e.g., effective fuel spraying, high temperature, optimal air-to-fuel ratio) and the different combinations of fuels used.

Because of the strong dependence of trace metals on rBC particles, one could expect that the sensitivity will also depend on the rBC mass loading present in the aerosol. In fact, the SP-AMS sensitivity drops as the rBC mass fraction decreases. That is, when the latter is low, the trace metal mass loadings are most likely not associated with rBC particles; trace metals will reside on non-rBC particles and are not detected via the laser vaporizer in the SP-AMS. As such, it does not matter how much rBC material would exist if the trace metals were not associated with these particle types. Thus, if we assume that trace metals and rBC are co-emitted, for instance in a combustion process, and if the trace metals exist on the rBC particle, if rBC is present, then the minimum amount of rBC necessary to detect the metals will be equal to or larger than the detection limit of rBC.

One method to investigate the sensitivity of the SP-AMS for trace metals is to estimate the limit of detection (LD).
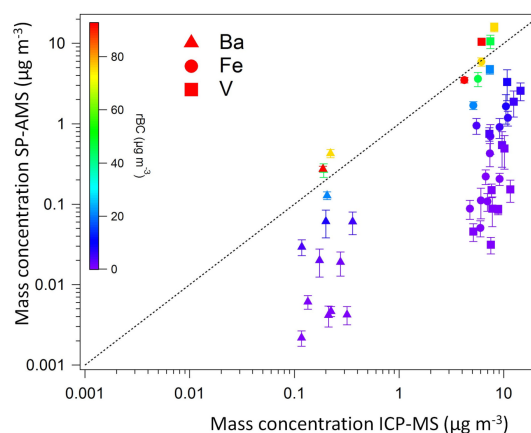
Figure 8. The metals barium, vanadium and iron measured with the SP-AMS vs. those collected with the NanoMOUDI and analyzed with the ICP-MS method (in $\mu g\, m^{-3}$) at the heating station.

LD was calculated by using 3 times the standard deviation of the metal concentration during a period when filtered air was measured (DeCarlo et al., 2006). The LD values were obtained as an average of 2 min measurements in 1 h of filtered air sampling during the experiment in the heating station. The LD values for metals varied between 10 (Sr^+) and 117 (Mn^+) ng m^{-3} (Table 2). During the same period, the LD of rBC was 13 ng m^{-3}. The latter was smaller than the value reported by Onasch et al. (2012) due to the different averaging time employed (1 min) but consistent with the Allan variance analysis. The presented limits of detection are relevant only for when the metals are on rBC aerosol particles.

3.2.5   Detection of metals in ambient particles

The detection of trace metals in ambient aerosol particles is limited to processes when trace metals are associated with rBC-containing particles. In fact, combustion emission processes such as vehicular exhaust, industrial and biomass burning emissions are common sources of ambient aerosol, typically co-emitting trace metals and rBC, which makes identification and quantification by the SP-AMS feasible.

Measurements in urban environments with this instrument showed the presence of the rBC in the Aitken and accumulation modes (Massoli et al., 2012) related to different sources with different mixing states (Lee et al., 2015). In the case of externally mixed particles, the detection of metals might be more limited. On the other hand, aged aerosol particles are often internally mixed, which may facilitate the detection of trace metals. For example in ambient measurement in Helsinki eight metals (Al, V, Fe, Zn, Rb, Sr, Zr and Cd) were detected with the SP-AMS, of which three (Sr, Zr and Cd) were detected only with the particle concentrator (Saarikoski et al., 2014).
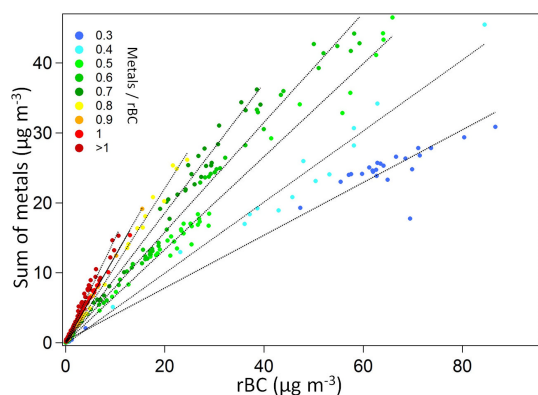
Figure 9. Mass concentration of the sum of all the metals measured at the heating station with the SP-AMS as a function of the rBC concentration.

4 Conclusions

A method for the detection and quantification of trace elements associated with rBC aerosol particles with the SP-AMS was presented. Quantification was achieved by obtaining the RIE values for 13 different metals relative to rBC. The method consisted of coating monodisperse rBC aerosol particles in trace metal standard solution; the rBC served as a carrier for the trace metals.

The values of RIE of each measured metal (RIE_{meas}) were compared to the literature RIE values (RIE_{theory}) and revealed similarity for those metals not significantly affected by the thermal surface ionization. The trace metals Rb, Na, Ba and Sr were thermally surface-ionized on the surface of the rBC particles, which enhanced their RIE values, compared to the theoretical values. Cu, Zn, V and Cr presented RIE_{meas} / RIE_{theory} values close to unity. The RIE_{meas} / RIE_{theory} ratio value for the transition metals Mn, Fe and Ni were lower than unity, likely due to processes such as losses.

In addition, the metals presented a negative mass defect in the mass spectrum that seemed to facilitate its identification and detection. However, because the metals are often present in low concentrations in ambient aerosol particles, their identification may be hampered by interference of other ions with larger signals. Therefore the use of the isotopes/isotopic composition for their quantification may be useful, e.g., ^{40}Ca and ^{42}Ca.

Moreover, in the laboratory experiment, size distribution information of each individual metal was achieved using the HR-PToF measurement indicating the presence of unimodal particle size distribution, which suggested that the metals were most likely attached to the rBC surface or interior. Trace metals were also investigated as a function of the laser current/power; a minimum current of 0.6 A, approximately 90 mW, was needed to fully vaporize the metals and the rBC.

The RIE values obtained in this study were tested in an oil-fired heating station in Helsinki. The concentrations of the Ba, V and Fe obtained with the SP-AMS were compared with the samples analyzed by the ICP-MS method. The comparison indicated good agreement for large concentrations of rBC (in raw flue gas). When the rBC mass loading decreased, the SP-AMS sensitivity to measure the trace metals dropped because the latter might reside on non-rBC-containing aerosol particles.

In addition, metallic salts such as vanadium sulfate, calcium sulfate, iron sulfate and barium sulfate were identified in the mass spectra of the emissions from the heating station. The presence of those salts resulted in a different sulfate fragmentation pattern than ammonium sulfate, the general form of sulfate in neutral ambient atmospheric aerosols.

Finally, the advantages of using the SP-AMS to measure trace metals, compared to other techniques (e.g., ICP-MS), range from real-time measurements to more detailed information on the characterization of metallic compounds, when those reside on rBC-containing particles. This instrument is especially recommended to study processes when the trace metals and the rBC are co-emitted, for instance combustion emission processes, such as vehicular, industrial and biomass burning.

The Supplement related to this article is available online at doi:10.5194/amt-8-4803-2015-supplement.

References

Alfarra, M. R., Coe, H., Allan, J. D., Bower, K. N., Boudries, H., Canagaratna, M. R., Jimenez, J. L., Jayne, J. T., Garforth, A., Li, S.-M., and Worsnop, D. R..: Characterization of urban and rural organic articulate in the Lower Fraser Valley using two Aerodyne aerosol mass spectrometers, Atmos. Environ., 38, 5745–5758, 2004.

Allan, J. D., Coe, H., Bower, K. N., Williams, P. I., Gallagher, M. W., Alfarra, M. R., Jimenez, J. L., Worsnop, D. R., Jayne, J. T., Canagaratna, M. R., Nemitz, E., and McDonald A. G.: Quantitative sampling using an Aerodyne Aerosol Mass Spectrometer. Part 2: Measurements of fine particulate chemical composition in two UK cities, J. Geophys. Res., 108, 4091, doi:10.1029/2002JD002359, 2003.

Allan, J. D., Delia, A. E., Coe, H., Bower, K. N., Alfarra, M. R., Jimenez, J. L., Middlebrook, A. M., Drewnick, F., Onasch, T. B., and Canagaratna, M. R.: A generalised method for the extraction of chemically resolved mass spectra from Aerodyne aerosol mass spectrometer data, J. Aerosol Sci., 35, 909–922, 2004.

Allen, A. G., Nemitz, E., Shia, J. P., Harrison, R. M., and Greenwood, J. C.: Size distributions of trace metals in atmospheric aerosols in the United Kingdom, Atmos. Environ., 35, 4581–4591, 2001.

Ago, H. Kugler, T., Cacialli, F., Salaneck, W. R., Shaffer, M. S. P., Windle, A. H., and Friend, R. H.: Work Functions and Surface Functional Groups of Multiwall Carbon Nanotubes, J. Phys. Chem. B, 103, 8116–8121, 1999.

Cross, E. S., Sappok, A., Fortner, E. C., Hunter, J. F., Jayne, J. T., Brooks, W. A., and Onasch, T. B., Wong, V. W., Trimborn, A., Worsnop, D. R., and Kroll, J. H.: Real-time measuremtns of engine-out trace elements: Application of a novel soot particle aerosol mass spectrometer for emissions characterization, J. Engin. for Gas Turbines and Power, 137, 072801, doi:10.1115/1.4005992, 2012.

Dallmann, T. R., Onasch, T. B., Kirchstetter, T. W., Worton, D. R., Fortner, E. C., Herndon, S. C., Wood, E. C., Franklin, J. P., Worsnop, D. R., Goldstein, A. H., and Harley, R. A.: Characterization of particulate matter emissions from on-road gasoline and diesel vehicles using a soot particle aerosol mass spectrometer, Atmos. Chem. Phys., 14, 7585–7599, doi:10.5194/acp-14-7585-2014, 2014.

DeCarlo, P., Slowik J. G., Worsnop, D. R., Davidovits, P., and Jimenez J. L.: Particle morphology and density characterization by combined mobility and aerodynamic diameter measurements. Part 1: Theory, Aerosol Sci. Technol., 38, 1185–1205, 2004.

DeCarlo, P. F., Kimmel, J. R., Trimborn, A., Northway, M. J., Jayne, J. T., Aiken, A. C., Gonin, M., Fuhrer, K., Horvath, T., Docherty, K. S., Worsnop, D. R., and Jimenez, J. L.: Field-deployable, high-resolution, time-of-flight mass spectrometer, Anal. Chem, 78, 8281–8289, 2006.

Dockery, D. W.: Epidemiologic Evidence of Cardiovascular Effects of Particulate Air Pollution. Environ. Health Persp., 109, 483–486, 2001.

EPA: Environmental Protection Agency, available at: http://www3.epa.gov/ttn/atw/nata2005/05pdf/2005polls.pdf, last access: June 2014, 2005.

Fabish, T. J. and Hair, M. L.: The Dependence of the Work Function of Carbon Black on Surface Acidity, J. Colloid Interf. Sci., 62, 16–23, 1977.

Fujii, K. and Srivastava, S. K.: A measurement of the electron-impact ionization cross section of sodium, J. Phys. E. At. Mol. Opt. Phys., 28, 559–563, 1995.

Freund, R. S., Wetzel, R. C., Shul, R., J., and Hayes, T. R.: Cross-section measurements for electron-impact ionization of atoms. Phys. Rev. A., 41, 3575–3595, 1990.

Frey, A. K., Saarnio, K., Lamberg, H., Mylläri, F., Karjalainen, P., Teinilä, K., Carbone, S., Tissari, J., Niemelä, V., Härinen, A., Rautiainen, J., Kytömäki, J., Artaxo, P., Virkkula, A., Pirjola, L., Rönkkö, T., Keskinen, J., Jokiniemi, J., and Hillamo, R.: Optical and Chemical Characterization of Aerosols Emitted from Coal, Heavy and Light Fuel Oil, and Small-Scale Wood Combustion, Environ. Sci. Technol., 48, 827–836, 2014.

Gao, Y., Nelson, E. D., Fielda, M. P., Ding, Q., Lia, H., Sherrella, R. M., Gigliotti, C. L., Van Ryb, D. A., Glenn, T. R., and Eisenreich, S. J.: Characterization of atmospheric trace elements on PM2.5 particulate matter over the New York–New Jersey harbor estuary, Atmos. Environ., 36, 1077–1086, 2002.

Happonen, M., Mylläri, F., Karjalainen, P., Frey, A., Saarikoski, S., Carbone, S., Hillamo, R., Pirjola, L.,Häyrinen, A., Kytömaäki, J., Niemi, J. V., Keskinen, J., and Rönkkö, T.: Size distribution, chemical composition and hygroscopicity of fine particles emitted from an oil-fired heating plant, Environ. Sci. Technol., 47, 14468–14475, 2013.

Jayne, J. T., Leard, D. C., Zhang, X., Davidovits, P., Smith, K. A., Kolb, C. E., and Worsnop, D. R.: Development of an aerosol mass spectrometer for size and composition analysis of submicron particles. Aeros. Sci. Technol., 33, 49–70, 2000.

Jimenez, J. L., Jayne, J. T., Shi, Q., Kolb, C. E., Worsnop, D. R., Yourshaw, I., Seinfeld, J. H., Flagan, R. C., Zhang, X., Smith, K. A., Morris, J., and Davidovits, P.: Ambient Aerosol Sampling with an Aerosol Mass Spectrometer, J. Geophys. Res.-Atmos., 108, 8425, doi:10.1029/2001JD001213, 2003.

Kim, Y., Migdalek, J., Siegel, W., and Bieron, J.: Electron-impact ionization cross section of rubidium, Phys. Rev. A., 57, 246–255, 1998.

Lee, A. K. Y., Willis, M. D., Healy, R. M., Onasch, T. B., and Abbatt, J. P. D.: Mixing state of carbonaceous aerosol in an urban environment: single particle characterization using the soot particle aerosol mass spectrometer (SP-AMS), Atmos. Chem. Phys., 15, 1823–1841, doi:10.5194/acp-15-1823-2015, 2015.

Liu, D.-Y., Rutherford, D., Kinsey, M., and Prather, K. A.: Real-Time Monitoring of Pyrotechnically Derived Aerosol Particles in the Troposphere, Anal. Chem., 69, 1808–1814, 1997.

Lotz, W.: Electron-impact ionization cross-sections for atoms up to $Z = 108$, Zeitschrift für Physik, 232, 101–107, doi:10.1007/BF01393132, 1970.

Lough, G. C., Schauer, J. J., Park, J.-S., Shafer, M. M., Deminter, J. J., and Weinstein, J. P.: Emissions of metals associated with motor vehicle roadways, Environ. Sci. Technol., 39, 826–836, doi:10.1021/es048715f, 2005.

Massoli, P., Fortner, E. C., Canagaratna, M. R., Williams, L. R., Zhang, Q., Sun, Y., Schwab, J. J., Trimborn, A., Onasch, T. B., Demerjian, K. L., Kolb, C. E., Worsnop, D. R., and Jayne, J. T.: Pollution Gradients and Chemical Characterization of Particulate Matter from Vehicular Traffic near Major Roadways: Results from the 2009 Queens College Air Quality Study in NYC, Aerosol Sci. Technol., 46, 1201–1218, 2012.

Mbengue, S., Alleman, L. Y., and Flament, P.: Size-distributed metallic elements in submicronic and ultrafine atmospheric particles from urban and industrial areas in northern France, Atmos. Environ., 135, 35–47, 2014.

Moffet, R. C., Desyaterik, Y., Hopkins, R. J., Tivanski, A. V., Gilles, M. K., Wang, Y., Shutthanandan, V., Molina, L. T., Abraham, R. G., Johnson, K. S., Mugica, V., Molina, M. J., Laskin, A., and Prather, K. A.: Characterization of aerosols containing Zn, Pb and Cl from an industrial region of Mexico City, Environ. Sci. Technol., 42, 7091–7097, 2008.

Naghma, R. and Antony, B.: Electron impact ionization cross-section of C_2, C_3, Si_2, Si_3, SiC and Si_2C. Molec. Phys., 111, 269–275, 2013.

Nilsson, P. T., Eriksson, A. C., Ludvigsson, L., Messing, M. E., Nordin, E. Z., Gudmundsson, A., Meuller, B. O., Deppert, K., Fortner, E. C., Onasch, T. B., and Pagels, J. H.: In-situ characterization of metal nanoparticles and their organic coatings using laser vaporization aerosol mass spectrometry, Nano Research, accepted, 2015.

Onasch, T. B., Trimborn, A., Fortner, E. C., Jayne, J. T., Kok, G. L., Williams, L. R., Davidovits, P., and Worsnop, D. R.: Soot Particle Aerosol Mass Spectrometer: Development, Validation, and Initial Application, Aerosol Sci. Technol., 46, 804–817, 2012.

Pacyna, J. M.: Source inventories for atmospheric trace metals, in: Atmospheric Particles, IUPAC Series on Analytical and Physical Chemistry of Environmental Systems, edited by: Harrison, R. M. and van Grieken, R. E., Wiley, Chichester, UK, 5, 385–423, 1998.

Prather, K. A., Nordmeyer, T., andf Salt, K.: Real-time characterization of individual aerosol particles using time-of-flight mass spectrometry, Anal. Chem., 66, 1403–1407, 1994.

Querol, X., Viana, M., Alastuey, A., Amato, F., Moreno, T., Castillo, S., Pey, P., de la Rosa, J., Sánchez de la Campa, A., Artinano, B., Salvador, P., Garcia Dos Santos, S., Fernandez-Patier, R., Moreno-Grau, S., Negral, L., Minguillon, M. C., Monfort, E., Gil, J. I., Inza, A., Ortega, L. A., Santamaria, J. M., and Zabalza, J.: Source origin of trace elements in PM from regional background, urban and industrial sites of Spain, Atmos. Environm., 41, 7219–7231, 2007.

Ramanathan, V. and Carmichael, G.: Global and Regional Climate Changes Due to Black Carbon. Nat. Geosci., 1, 221–227, doi:10.1038/ngeo156, 2008.

Saarikoski, S., Carbone, S., Cubison, M. J., Hillamo, R., Keronen, P., Sioutas, C., Worsnop, D. R., and Jimenez, J. L.: Evaluation of the performance of a particle concentrator for online instrumentation, Atmos. Meas. Tech., 7, 2121–2135, doi:10.5194/amt-7-2121-2014, 2014.

Salcedo, D., Laskin, A., Shutthanandan, V., and Jimenez, J. Feasibility of the detection of trace elements in particulate matter using online high-resolution aerosol mass spectrometry, Aeros. Sci. Technol., 46, 1187–1200, 2012.

Shiraishi, M. and Ata, M.: Work function of carbon nanotubes, Carbon, 39, 1913–1917, 2001.

Stephens, M., Turner, N., and Sandberg, J.: Particle identification by laser-induced incandescence in a solid-state laser cavity, Appl. Optics, 42, 3726–3736, 2003.

Su, Y., Sipin, M. F., Furutani, H., and Prather, K. A.: Development and characterization of an aerosol time-of-flight mass spectrometer with increased detection efficiency, Anal. Chem., 76, 712–719, 2004.

Sueper, D.: ToF-AMS High Resolution Analysis Software – Pika, available at: http://cires.colorado.edu/jimenez-group/wiki/index. php/ToF-AMSAnalysisSoftware (last access: June 2014), 2008.

Todd, J. F. J.: Recommendations for nomenclature and symbolism for mass spectroscopy, Pure Appl. Chem., 63, 1541–1566, 1991.

Vainshtein, L. A., Ochkur, V. I., Rakhovskii, V. I., and Stepanov, A. M.: Absolute values of electron impact ionization cross sections for magnesium, calcium, strontium and barium, Soviet Phys. Jet P., 61, 511–519, 1972.

Watson, P. R., Van Hove, M. A., and Hermann, K.: NIST Surface Structure Database – Ver. 5.0 National Institute of Standards and Technology, Gaithersburg, MD, 18 pp., 2004.

Willis, M. D., Lee, A. K. Y., Onasch, T. B., Fortner, E. C., Williams, L. R., Lambe, A. T., Worsnop, D. R., and Abbatt, J. P. D.: Collection efficiency of the soot-particle aerosol mass spectrometer (SP-AMS) for internally mixed particulate black carbon, Atmos. Meas. Tech., 7, 4507–4516, doi:10.5194/amt-7-4507-2014, 2014.

Zandberg, E. Y. and Ionov, N. I.: Surface Ionization (translated from Russian), Israel program for scientific translations, Israel Program for Scientific Translations, Jerusalem, 355 pp., 1971.